A STUDY ON THE VACUUM ULTRAVIOLET RADIATION FROM LASER-PRODUCED PLASMAS

Håkan Pettersson

LRAP-92

PREFACE

This is a diploma work made at the Department of Atomic Physics at Lund Institute of Technology. The purpose of this work was to examine VUV-radiation from laser-produced plasmas. When a powerful laser beam is focused on a target a plasma is produced due to the extreme energy density. Very high plasma temperature can be obtained. The plasma temperature raises to about 10^5 K in a few nanosecs. The plasma emits radiation within a broad wavelength interval from soft x-ray to infra-red. The influence on the radiation with respect to different materials in the target and laser power have been examined. Two different radiation detection systems have been used. For relative intensity measurements was an ordinary monochromator combined with a photomultiplier used. To be able to measure the absolute intensity (i.e. the number of photons), an ionization chamber was used. All calculations have been put in separate appendices but all important results are presented in the text.

I would like to thank my supervisor Dr. Hans Lundberg and Hans Hallstadius M.Sc.tech. for their help in conducting this diploma work. I am also most grateful to Dr. Stig Borgström and Dr. Ulf Litzén for all their help. I would also like to thank the workshop personel for all invaluable assistance.

Lund, Mars 1988

Håkan Pettersson

CONTENTS

1 INTRODUCTION

With the introduction of the laser to the laboratory as a high-power source of coherent radiation a new window to high-energy physics was opened. Of course, a considerable interest in the interaction between radiation and matter was born. The development of Q-switched lasers provided the advantage of a single light pulse with an extreme energy density. Accordingly, much of the interest was concentrated on various aspects of the hot, dense plasmas which were readily produced by a laser beam focused on a solid target.

The hot plasma will emit radiation which consists of two parts. One continous part, often referred to as blackbody radiation, and one discrete part, known as line radiation. This will be discussed more in the next chapter, which is more theoretical.

Why is this radiation important to study? Well, it may be used , for example, as a pump source in short wavelength lasing systems, and in applications as photolithography, microscopy and biochemistry. The radiation is also used for spectroscopy in atomic and molecular physics.

2 THEORETICAL BACKGROUND

2.1 Plasma theory

Studies of matter in outerspace have shown that besides solids, liquids and gases a fourth state of aggregation has to be acknowledged. This fourth state is known as a plasma. A plasma is a mixture of neutral atoms, electrons, ions and quantums emitted from atoms or ions. The plasma as a whole is electrical neutral. A plasma can be created by an electric discharge through a gas. Another way is by focusing a laser beam on a solid target. Due to the high-energy density the solid vaporizes. The vapor absorbs more energy until a plasma is formed.

There is a great difference in the behaviour of surfaces struck by laser pulses with millisecond durations as compared to those with pulse durations in the nanosecond region [ref. 1]. Typically, very high power short pulses do not produce much vaporization from the surface, whereas longer, lower power pulses from a normal pulse laser produce deep, narrow holes in the material. Another important thing is that the metal surface does not reflect the radiation from high power short pulses. The spiking behaviour of the laser will also influence the vaporization. In my case a Q-switched Nd:YAG laser with a ten nanosecond pulse duration is used, which gives a flux density around $10^{16} W/m^2$. With this flux density one cannot neglect the interaction between the vapor and the target. The vapor exerts a high pressure on the surface, which changes the vaporization characteristics of the surface. The vapor can absorb light and shield the surface from the laser light. It is the latter effect that produces extremely hot plasmas.
Near the beginning of the laser pulse, the surface absorbs the laser radiation and begins to vaporize. In the flat region which extents throughout most of the pulse time the plasma in front of the surface is absorbing and vaporization of the surface ceases. Near the end of the laser pulse the plasma is so hot that it reradiates energy and the surface again starts to vaporize. Thus, a given amount of energy delivered at very high power is less effective in causing vaporization than the same amount of energy delivered in a longer, lower power pulse.

The time behaviour of the depth vaporized by a Q-switched laser pulse can be as shown schematically in figure 2.1.1.

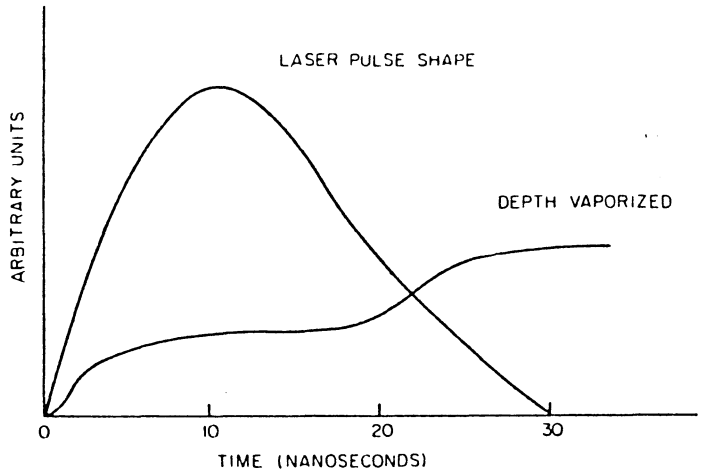

Fig.2.1.1 Schematic representation of the depth vaporized in a metal target as a function of time. A high-flux density pulse with the indicated pulse length was used [taken from ref.1].

The absorption of laser radiation in the blowoff material is due to the invers bremsstrahlung process [ref.1] as long as the energy density not exceeds about $10^{17}W/m^2$(my case). When the energy density do exceed $10^{17}W/m^2$ the absorption process is quite different. This is because bremsstrahlung absorption is essentially due to electrons oscillating in the electric field of the light wave. The electrons collide with ions via the coulomb forces, and so the absorption depends on the electron-ion collision frequency. The collision frequency is proportional to $T^{-3/2}$. A hot plasma is thus essentially collisionless. Instead the incident wave excites plasma waves (plasmons), which delivers energy (collisionless) to the electrons. The invers bremsstrahlung process involves absorption of a photon by a free electron. In this excitation the electron is raised to a higher state in the continuum available to it. The process must take place within the field of an ion in order to conserve momentum. This is called an inverse free-free transition, since the electron is free before and after the transition.

The absorption coefficient k_ν is given in cgs units by

$$k_\nu = 4/3(2\pi/3)^{1/2}(mkT)^{-3/2}n_e n_i Z^2 e^6/c\nu^2 \qquad (2.1)$$

where n_e and n_i are, respectively, the electron and ion densities in the plasma of average charge Z and temperature T. ν is the frequency of the light and c, e, m and k are, respectively, the velocity of light, the electronic charge, the electronic mass and the constant of Boltzmann. This means that radiation will be absorbed in a dimension of $1/k_\nu$. Efficient heating therefore requires that the plasma is of dimension $1/k_\nu$. The plasma will not be heated uniformly if the dimension of it exceeds the absorption length. On the other hand, energy will be wasted if the plasma dimension is smaller than the absorption length. Penetration into the plasma requires that the optical frequency ν_p must be higher than the collective oscillation frequency of the electrons with respect to the ions [ref.3]. The latter frequency is referred to as the plasma frequency and is given by

$$\nu_p = 56.4n_e^{1/2} \qquad (2.2)$$

where n_e is the electron density in the plasma. At higher electron density the plasma will reflect the incident radiation. The rapid expansion of the blowoff material means that the density would quickly drop below the critical value. The plasma frequency refers to one example of resonant type phenomena. Others, with different characteristic frequencies, may occur if the incident waves match a linear combination of these frequencies. Energy transfer from laser radiation to plasma is then enhanced. The plasma lasts essentially the same length of time as the exciting pulse.

There have been many investigations of plasma production by a variety of techniques such as optical methods, charge collection methods and mass spectroscopic methods [ref.1]. Optical spectroscopic studies on plasmas show, as mentioned before , both line and continuum radiation.

The line radiation originates at some distance from the target. It shows that highly ionized stages are present [ref.1]. Experimental work has shown that the higher stages of ionization are observed much earlier and last for a shorter time than the lower stages. A common feature of the spectra is also that at the very-high power levels the lines observed arise mainly from two

adjacent ionization stages. Those from lower stages are almost absent. This can be understood by taking the Saha equations in consideration. The Saha equations describe the populations of the ionization states in a plasma in local thermodynamic equilibrium at a temperature T

$$\frac{N_e N^z}{N^{z-1}} = \frac{2Z^z(T)}{Z^{z-1}(T)}\left(\frac{2\pi mkT}{h^2}\right)^{3/2} \exp\left(-\frac{E^{z-1} - \Delta E^{z-1}}{kT}\right), \qquad (2.3)$$

where m, k and h are the electron mass, the constant of Boltzmann and the constant of Planck, respectively. N^z/N^{z-1} is the ratio of the densities of atoms in states z and z-1, N_e is the electron density, E^{z-1} is the ionization energy of state z-1 for isolated atoms and ΔE^{z-1} is a correction factor for interactions in the plasma. The form of equations represented by (2.3) is such that at a high temperature one or more ionized species dominates. The formula above holds only for local thermodynamic equilibrium (LTE), which means that collisional excitation and energy transfer processes are sufficiently rapid. The equipartition time for transfer of energy from electrons to ions is short. This time is given experimentally by

$$t = 25.2AT^{3/2}/n_e Z^2, \qquad (2.4)$$

where A is the atomic weight of the ions. For Q-switched lasers t will often be shorter than the duration. For picosecond laser systems this may not hold. Thus, only for Q-switched laser pulses is LTE a satisfactorial approximation. High electron density is desirable to produce equilibrium quickly. The electron and ion temperature at LTE may be regarded as equal.

The continuum radiation originates near the target surface and covers most of the spectral range from 20 to 6000 Å. In my case only the VUV range (i.e. 300 to 2000 Å) is studied. The continuum radiation generally consists of bremsstrahlung and recombination radiation. Bremsstrahlung is the emission of a photon as an electron, influenced by the field of the ions, is deexcited to a lower state in the continuum available to it. The rate of emission of bremsstrahlung per frequency intervall from a unit volume is [ref. 4]

$$P^B(\nu)d\nu = Cg_{ff} n_e n_z Z^2 (kT_e)^{-1/2}/(2X_0) \exp(-h\nu/kT_e)d\nu, \qquad (2.5)$$

where C, g_{ff}, n_e, n_z and X_0 are, respectively, $6.2\pi e^4 h X_0^{3/2}/m^2c^3$, the free-free

Finally, I would like to schematically (figure 2.1.2) show what is occuring in a plasma, which is pumped by a Q-switched laser pulse, at some typical time t in the pulse [ref.3].

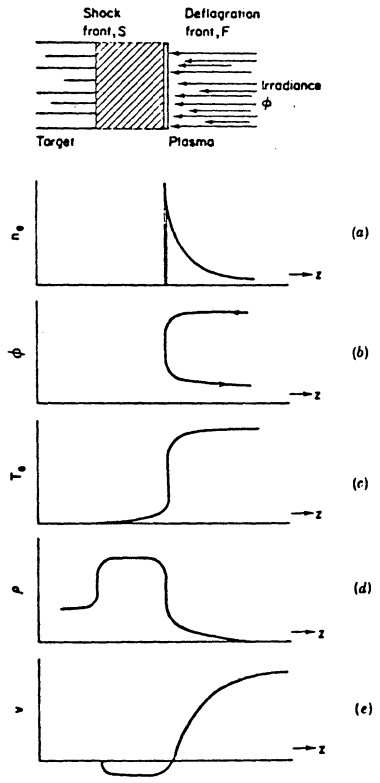

Fig.2.1.2 Conditions after a time t at a semi-infinite block target subject to constant radiation Φ:
(a) electron density
(b) intensity of incident and reflected radiation
(c) electron temperature
(d) density and (e) velocity
all as functions of distance z from target. The ordinate scales are all arbitrary [taken from ref.3].

Figure 2.1.2 shows the position of the target surface before irradiation begins. The deflagration zone may be considered as the seat of the energy which drives the processes in, and associated, the plasma. The deflagration front, F, travels into the target with a velocity v_f and the shock front S with velocity v_s. To the left of S we have the undisturbed solid and to the right of F the expanding plasma. Figure 2.1.2(a) shows the electron density and indicate as the deflagration zone the region over which n_e falls from n_c, if n_c is assumed to be attained, to $0.9n_c$. The most energy will be delivered here. The intensity variation of the incoming and outgoing radiation after reflection at the critical layer, shown in figure 2.1.2(b), illustrates this point further. Figure 2.1.2(c) shows the temperature profile. It raises sharply at the deflagration front and is assumed to be constant in the streaming plasma. Conductivety across the target surface is found to be so small that the temperature drops rapidly. Figure 2.1.2(d) shows the density profile. Note, how the shockwave increases the density of the target. Finally, figure 2.1.2(e) illustates the velocity profile for the entire system.

2.2 Theory of absolute intensity measurements

To measure the absolute intensity of radiation of any wavelength a detector, whose response is known in absolute units, must be used. The detector must either be calibrated against a standard source of known intensity or it must be an absolute detector, whose response to the intensity of radiation can be predicted [ref.5].

Because of the lack of absolute detectors, intensity measurements have in the past been based on absolute sources of radiation such as the ideal blackbody furnace. Secondary standard sources are then constructed and calibrated against the primary blackbody source. These secondary standard sources are typically specially constructed tungsten filament lamps produced by the National Bureau of Standards. The emission of these lamps is confined to wavelengths longer than 2700 Å. To measure absolute intensities at shorter wavelengths, it is necessary to select a stable detector whose response is constant with respect either to wavelength or frequency since the detector must be calibrated at longer wavelengths. One way to construct an absolute detector is by utilizing the principle of photoionization of a rare gas. Over a certain wavelength range, every photon absorbed by the gas produces an electron-ion pair. If total absorption of the light occurs the number of photons incident on the gas is simply equal to the ion current produced. The long wavelength limit of such an absolute detector is 1022 Å, the ionization potential of xenon. The short wavelength limit using helium is about 250 Å. For shorter wavelengths the ejected photo electrons have enough energy to produce secondary ionization. This phenomena, of course, gives an incorrect signal. The ionization potentials of the rare gases are given in table 2.1.

Table 2.1 Ionization potentials of the rare gases [taken from ref.5].

	Ionization Potential (Å)	
Gas	$^2P_{3/2}$	$^2P_{1/2}$
He	504.26	
Ne	574.93	572.37
Ar	786.72	777.96
Kr	885.62	845.42
Xe	1022.14	922.75

Actually, any gas would suffice provided its photoionization yield is known. The photoionization yield of a gas is defined as the number of ions produced per photon absorbed by the gas. All polyatomic gases have, in general, yields which are equal to or less than 100 per cent. One reason for yields less than 100 per cent is that the photon energy may be absorbed in dissociating the molecule and leaving some or all of the constituent atoms in excited states. Atoms, on the other hand, have normally yields of 100 per cent. The interaction between the continuum and the discrete atomic levels usually results in radiationless transitions into the continuum with the release of a photo electron. This process is called autoionization (Augereffect). The ratio of the number of photo electrons emitted to the total number of atoms excited into an autoionized state is equal to $\alpha/\alpha+\beta$, where α and β are the probabilities for radiationless and radiative transitions, respectively. The sum of transition probabilities is equal to the inverse of the mean lifetime of that state. Since, the probability of radiationless transitions into the ionization continuum is commonly of the order of 10^{13} s^{-1} to 10^{15} s^{-1} compared to 10^{8} s^{-1} for a radiative transition, then $\alpha/\alpha+\beta$ is essentially unity. Thus, the photoionization yield of an atom is expected to be unity in an autoionized state.

The rare gases are our only source of permanent atomic gases. The photoionization yields of these gases are shown to be 100 per cent. Thus, if an ionization chamber is constructed and filled with the appropriate rare gas until all of the incident radiation is absorbed, then the number of photons per second incident on the gas is simply equal to the ion current produced.

There exists several designs of ionization chambers. A standard one is shown in figure 2.2.1.

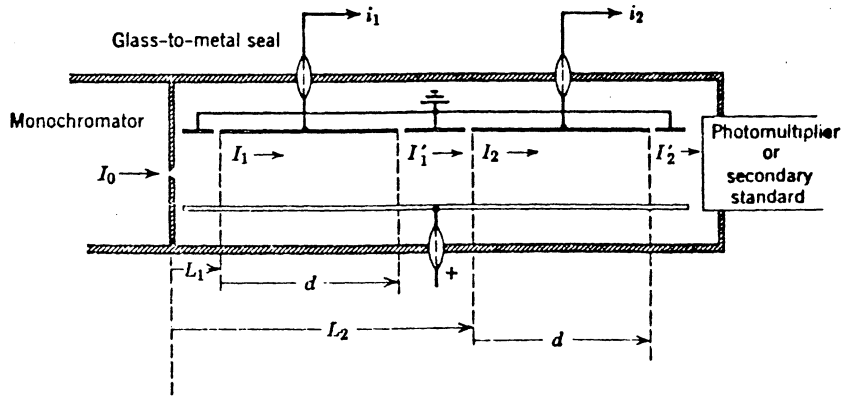

Figure 2.2.1 Double ionization chamber [taken from ref.5].

Denote I_0 as the incident light intensity to be measured; then with a gas in the cell at some suitable pressure, say p, denote I_1 and I_1' as the intensities entering and leaving plate 1, and denote I_2 and I_2' as the intensities entering and leaving plate 2. The three small plates alternating with the ion collection plates are guard rings to provide a uniform field between the parallell plates. The repeller plate is held at a few volts positive to drive the ions to the collector plates 1 and 2. Now at plate 1, the total number of ions produced per second is equal to i_1/e where i_1 is the electronic current in amperes and e is the electronic charge measured in coulombs. The total number of photons absorbed per second is equal to (I_1-I_1'). Using Lambert's law, this becomes

$$I_1-I_1' = I_0e^{-\mu L_1}(1-e^{-\mu d}), \tag{2.10}$$

where μ is the absorption coefficient of the gas measured at a pressure p; L_1 and d are the dimensions shown in figure 2.2.1. From the definition of the photoionization yield we get

$$\gamma = \frac{i_1/e}{I_0e^{-\mu L_1}\ (1-e^{-\mu d})}. \tag{2.11}$$

Similarly for plate 2

$$\gamma = \frac{i_2/e}{I_0e^{-\mu L_2}\ (1-e^{-\mu d})} \tag{2.12}$$

From the ratio of (2.11) and (2.12) and solving for μ we get

$$\mu = \ln(i_1/i_2)/(L_2-L_1). \tag{2.13}$$

Substituting μ into (2.11) and assuming $\gamma = 1$ gives

$$I_0 = \frac{i_1/e}{e^{-\ln(i_1/i_2)L_1/(L_2-L_1)}\ (1-e^{-\ln(i_1/i_2)d/(L_2-L_1)})}. \tag{2.14}$$

The major advantage of the double ionization chamber lies in the fact that all the variables, namely the two ion currents, can be measured simultaneously. Discrepancies due to light fluctuations are thereby eliminated.

The use of photoionization techniques for absolute intensity measurements requires some care. Since a gas flow through the ionization chamber is necessary, pressure gradients may occur. These would be detrimental when using

a double ionization chamber. Another problem is, since we do not use any windows in this spectral region, to maintain high vacuum in the cells connected to the ionization chamber. The first problem is reduced by using a large diameter ionization chamber with a very small entrance slit. The second problem is reduced by using a rather long ionization chamber, so that less gas pressure is required to absorb the incident radiation.

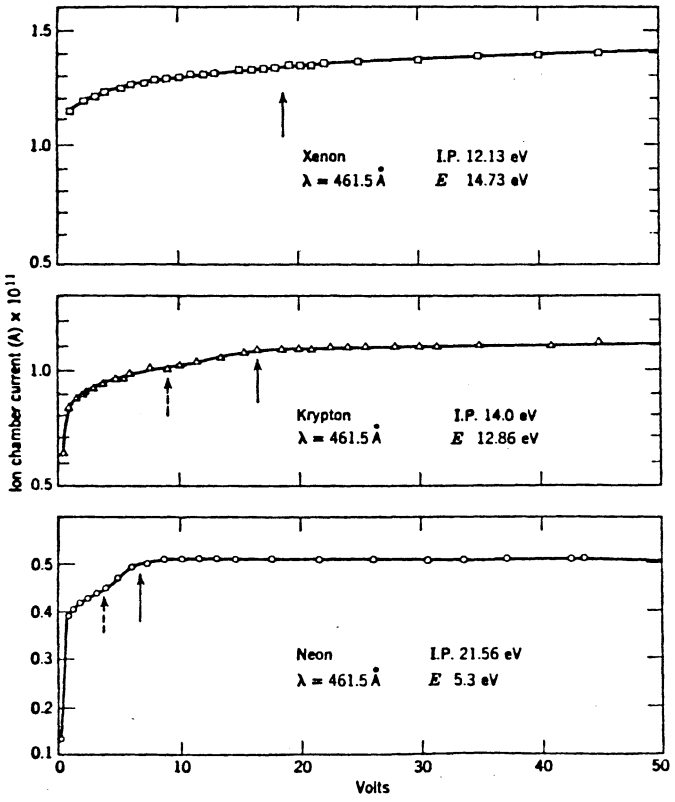

Fig.2.2.2 Ionization chamber currents as a function of voltage for Xe, Kr and Ne at 461.5 Å. In each case, the dashed vertical arrow indicates the voltage necessary to commence electron retardation whereas the solid arrow indicates the voltage necessary to complete electron retardation. E represents the energy of the ejected electron due to radiation of wavelength λ [taken from ref.5].

Probably one of the most important precautions to take is in using a proper collector voltage; that is, we must operate in the plateau region of the ions

versus voltage curve. This is to make sure that all produced ions are collected. For example, if xenon was ionized by 461.5 Å (26.9 eV), an electron could be ejected with an energy E given by

$$E = h\nu - I(Xe), \qquad (2.15)$$

where I(Xe) is the ionization potential of xenon (12.1 eV) and $h\nu$ is the energy of the incident photon, in this case 26.9 eV. Substituting these values into (2.15) gives E = 14.8 eV. Thus, the electron is emitted with sufficient energy to cause secondary ionization. With the addition of a collector voltage, this energy is increased. It is, therefore, impossible to achieve a plateau with xenon at 461.5 Å. The top curve in figure 2.2.2 illustates this point for a particular ionization chamber.

The collection of electrons as well as ions may occur if an insufficiently high electron retarding potential is used. The dependence on the ion current due to collected electrons is illustrated in figure 2.2.2.

3 EXPERIMENTAL SETUPS

3.1 Discussion

To examine the frequency distribution of radiation in general, all we need is a grating and some kind of quantum detector. Examples of these are the photomultiplier and the photoconductive semiconductor.
However, when the wavelength falls below 180 nm, air begins to absorb the radiation. To evade this problem we have to place the source and all the equipment in a vacuum system.
As shown in figure 3.1.1 the VUV-region extends far below 180 nm. Therefore, I had to work at a pressure nearby vacuum.

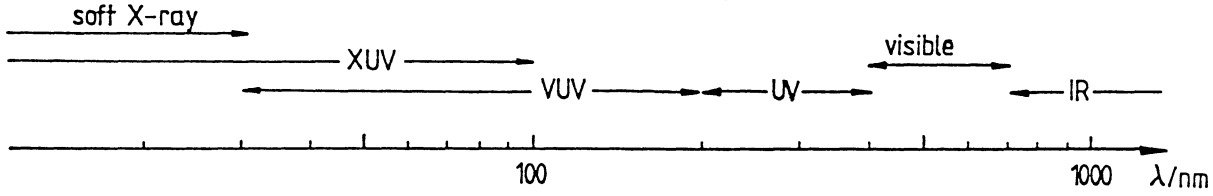

Fig 3.1.1 Designation of spectral regions [taken from ref. 2].

I used two different detection methods, which are described in the next two subchapters:
1) Monochromator with a photomultiplier.
2) Ionization chamber.

3.2 The monochromator-photomultiplier arrangement

The experimental arrangement is shown in figure 3.2.1.

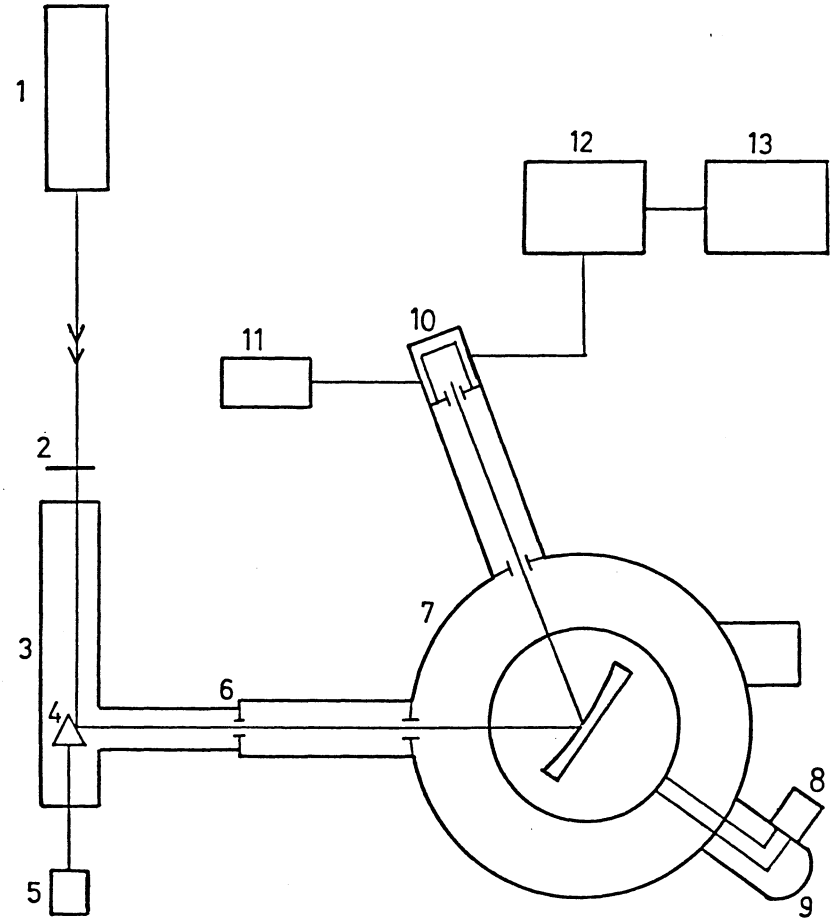

Fig. 3.2.1 The setup

(1) Nd:YAG laser
(2) Focusing lens
(3) Target chamber
(4) Target
(5) A.C motor
(6) Entrance slit
(7) Monochromator
(8) Motor with gearbox
(9) Vacuum pump connection
(10) Photomultiplier
(11) PMT power supply
(12) Boxcar integrator
(13) Printer

The laser beam (1.06 μm) was focused by a 10-inch lens onto the target. The target chamber consists of a tube made of stainless steel. It has four connections, one of which fits onto the monochromator entrance. Opposite the

monochromator there is a inspection window mounted. In the end pointing towards the laser there is a quartz window mounted. To make sure that reflections in the window are harmless, the window is angled somewhat downwards. A sealed passage for a rotating shaft is mounted on the other end. The target was glued to the drive shaft. The shaft rotated about 1 r/s. Three different target materials were used (W, Ta and Al). The target had the shape of a cone. The laser beam hit the target on the mantle. By doing this the radiation from the plasma was less shielded by the walls surrounding the risen pit.

The radiation from the plasma entered the monochromator via an entrance slit. The monochromator was constructed at Fysicuum, Uppsala, on the pattern of a McPherson model. The angle between the monochromator arms is 70.15^{0} and their lengths are 80 cm. They are exchangeable into two arms of half length, depending on which grating is used. The monochromator is evacuated to a pressure of about 10^{-5} torr by an oil diffusion pump, with a capacity of 80l/s. A trap with liquid nitrogen can be connected to the diffusion pump. If so, the pressure can be reduced to about 10^{-7} torr. A rotary pump is working on the exit of the diffusion pump. The widths of the entrance and exit slits are fixed, but they are easily exchanged.

The original grating is made by Bausch & Lomb. It is a concave grating with a focal length of 0.5 m, 600 lines per mm and a blaze at 1200 Å. It is usable for wavelengths down to 600 Å, where the reflectivity drops dramatically. A new grating with a focal length of 0.25 m, 1200 lines per mm and a blaze at 700 Å is procured. According to the manufacturer, this grating is usable down to 300 Å.

The adjustment unit of the grating consists of a micro-meter screw for the coarse adjustment, located on the grating table inside the monochromator, and a motordrive unit which is operated from the outside. The scale on the motor runs from about 50 to 900 units. The correlation between a scale unit, for different adjustments on the micro-meter screw, and the wavelength for the original grating is shown in figure 3.2.2. A corresponding correlation for the new grating is shown in figure 3.2.3.

The photomultiplier is made by Hamamatsu. It is of an open type. The spectral range is 300-1400 Å, with a response peak at about 700 Å. The rise time is 10 ns and it should be supplied with around 2400 V.

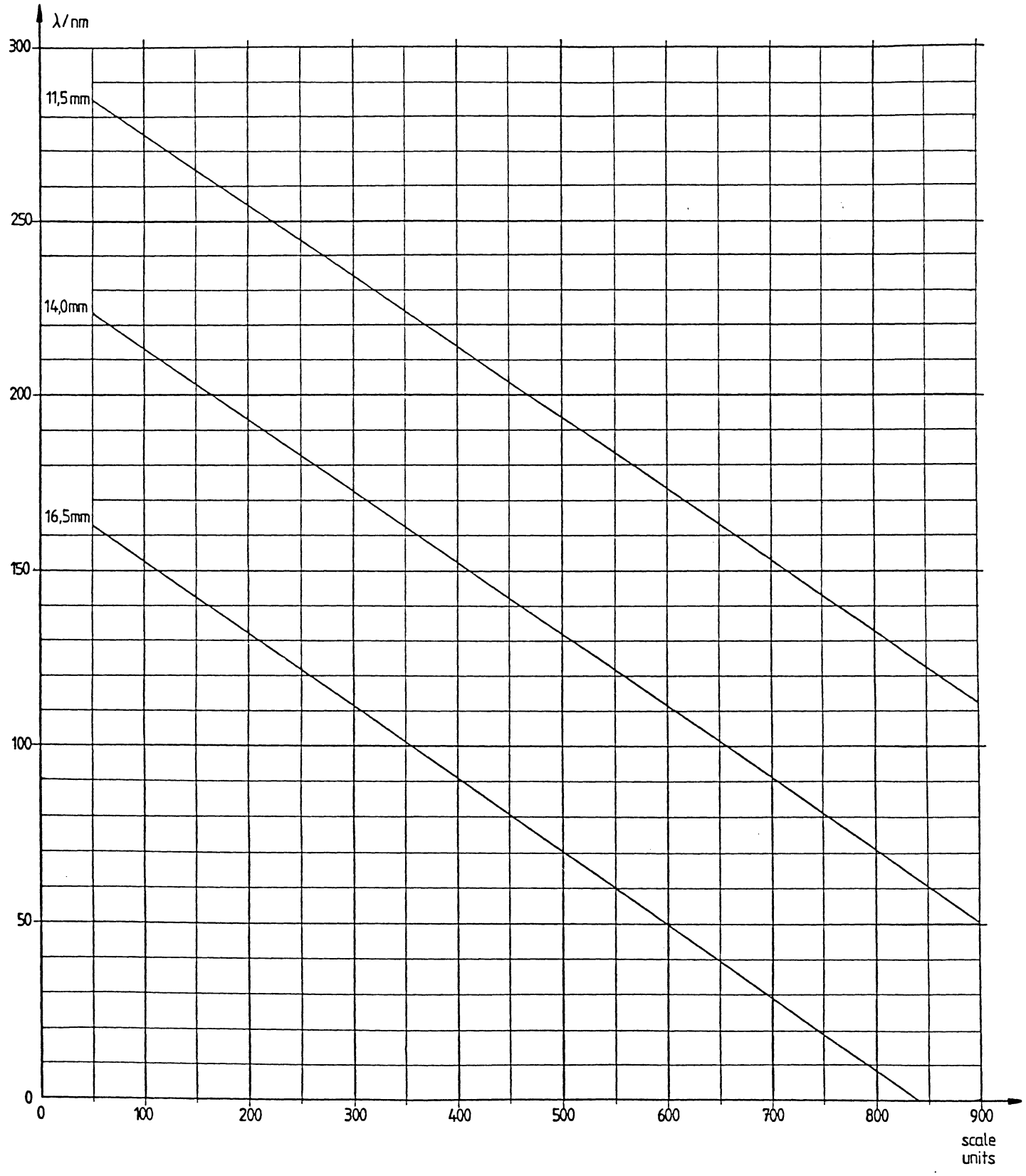

Fig.3.2.2 Correlation between scale units and wavelength for the original grating.The micro-meter screw settings are 11.5,14.0 and 16.5 mm. [taken from ref.2].

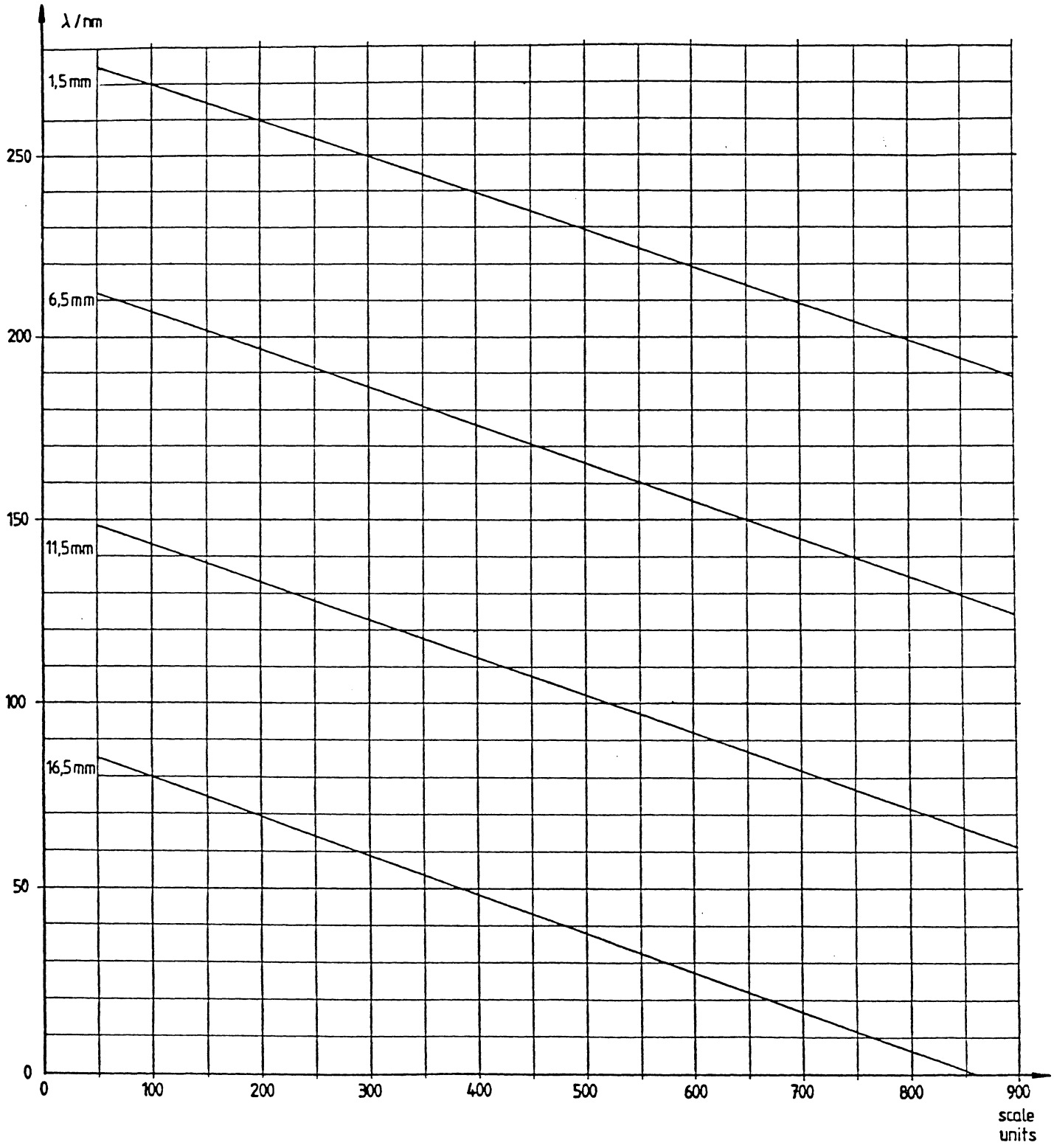

Fig. 3.2.3 *Correlation between scale units and wavelength for the new grating. The micro-meter screw settings are 1.5, 6.5, 11.5 and 16.5 mm [taken from ref. 2].*

3.3 The ionization chamber arrangement

The experimental arrangement is shown in figure 3.3.1.

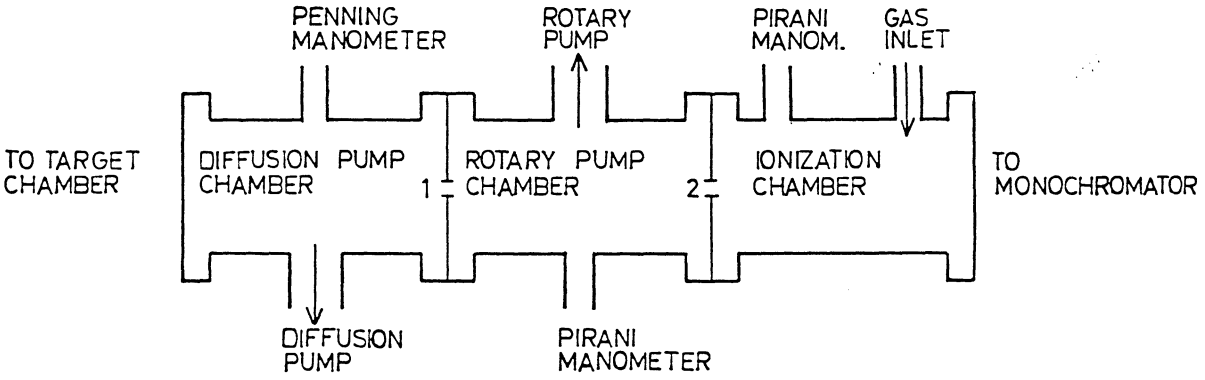

Fig.3.3.1 The differential pumping and ionization chamber system.
(1) Slit 1x8mm^2
(2) Slit 0.5x3mm^2

The ionization chamber is made of stainless steel. It contains a unit of three parallel copper plates, placed in two tracks which are milled in two pieces of teflon. The distance between the copper plates is 8 mm. There are two BNC-connections on each side of the ionization chamber. The ionization chamber is isolated from ground via teflon plates. Figure 3.3.2 shows the electrical setup for the ionization chamber.

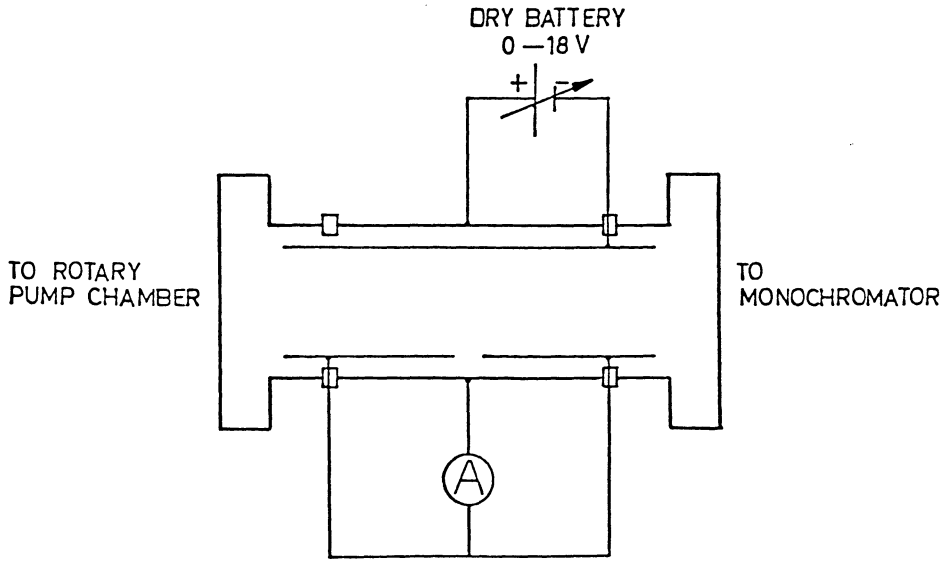

Fig.3.3.2 The electrical setup

There are two pumpchambers in the system. They are both also made of stainless steel. One is connected to an efficient rotary pump. The other is evacuated by an oil diffusion pump, with a capacity of 80 l/s. These chambers are necessary when the wavelengths are shorter than the MgF_2-cutoff at 1120 Å and a open, differentially pumped system is the only solution.

4 THE EXPERIMENTS AND RESULTS

4.1 Relative intensity measurements

The experimental arrangement shown in figure 3.2.1 was set up. The new grating with characteristics described in subchapter 3.2 was used in the following experiments. When the pumps had evacuated the monochromator to about 10^{-5} mbar the Nd:YAG laser was turned on. The voltage to the photomultiplier (~ 2400 V) was also turned on. To optimize the signal from the photomultiplier, that is, to make sure that the focused laser beam hit the target aligned with the monochromator entrance slit the target as well as a couple of laser mirrors were adjusted until a maximum signal was indicated on the printer. The grating was turned until the scale on the motor showed 50. The correlation between scale units and wavelength is shown in figure 3.2.3. The experiments could begin.

Changes in the radiation emitted from the plasma due to varying laser power, with target materials W, Ta and Al, was to be examined.

The radiation from the plasma was examined for two values of the laser energy output (0.15 J and 0.65 J). The calculation of the corresponding values for the power densities is shown in appendice A1.

Unfortunately, these experiments were not successful. The continuum radiation had a maximum at about 400 Å. The photomultiplier response at this wavelength was vanishing. The results were therefore heavily distorded.

Fortunately, Dr. Ulf Litzén could provide us with results from similar experiments. His equipment consisted of a huge monochromator with a gold coated grating, provided with 1200 lines per mm. The grating was mounted on a Rowland circle with a radius of 3 m. The incidence angle was 10^{0}. He used photographic registration, which is more linear than a photomultiplier. A micro-densitometer transferred the blackening on the photographic plate into relative intensities. The power source was a Nd:YAG laser.

The pulse energy was 0.8 J. The target material was tungsten. The result from the experiment is shown in figure 4.1.1.

The maximum intensity was located at about 400 Å. In another experiment, the result of this is not presented here, we raised the pulse energy to 2.5 J. The wavelength corresponding to the maximum intensity did not alter. The conclusion of this may be that the continuum radiation consisted mainly of recombination radiation. This makes it difficult to estimate the

plasma temperature. However, a temperature of 1.5×10^5 K - 2.0×10^5 K sounds reasonable. Noticable in figure 4.1.1 is also the lack of strong line radiation.

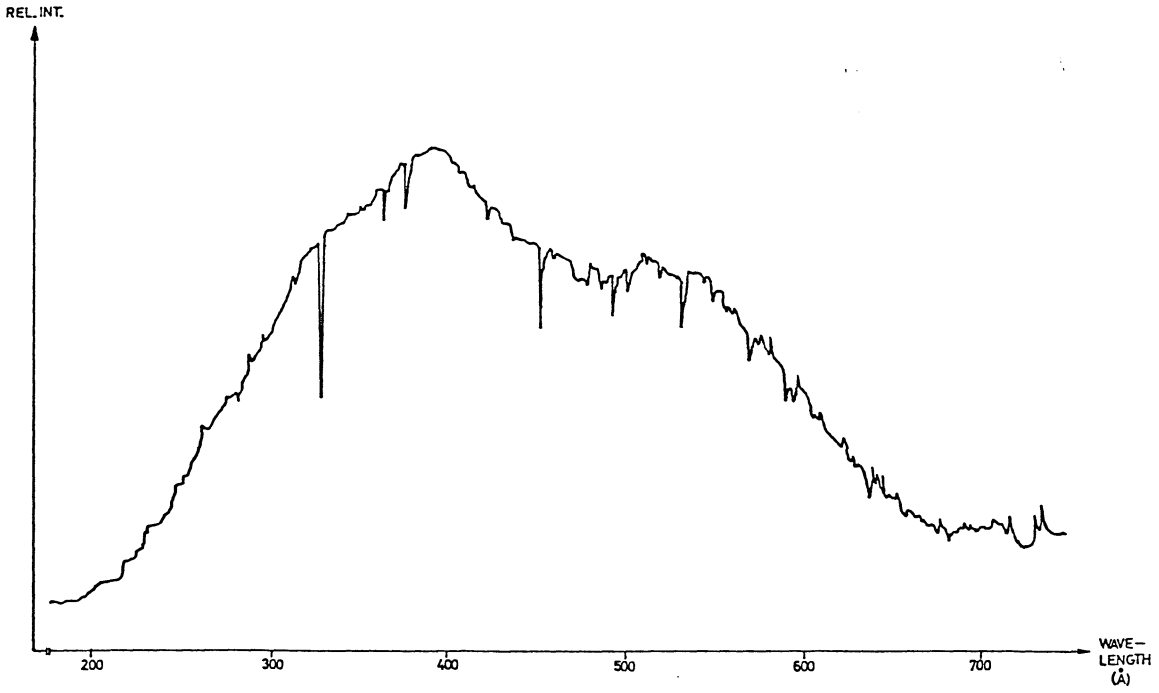

Fig. 4.1.1 The relative intensity from a tungsten plasma which is pumped by a 0.8 J pulse from a Nd:YAG laser.

4.2 Absolute intensity measurements

A theoretical background to this part is given in subchapter 2.2. After constructing the ionization chamber the drawings were sent to the workshop. When the skilled mechanics were ready the experimental arrangement shown in figures (3.3.1 and 3.3.2) was set up. A noble gas was flowed through the ionization chamber and a few volts were put across the copper plates. The Nd:YAG laser was turned on. The induced ion current from the ionization chamber was registered on a very sensitive Knick nanoamperemeter. To optimize this signal, that is, to make sure that the focused laser beam hit the target aligned with the ionization chamber entrance slit a similar adjustment to the one described in subchapter 4.1 was done. The target material was tantalum. Now the actual experiments could start.

Three different experiments were to be performed:
1) The voltage influence on the ion current.
2) The noble gas pressure influence on the ion current.
3) The laser power output influence on the ion current.

Experiment 1:
This was made only for one noble gas (argon), since the general appearance of the diagram ought to be the same for all noble gases. After choosing a suitable pressure the voltage was continously changed from 0 - 18 V, as the ion currents were registered. The result is shown in figure 4.2.1.
A voltage plateau is seen at voltages above 5 volts. Interesting is also the remaining ion current at zero volts. This is because some ions will strike the cathode even without a guiding electric field.

Experiment 2:
Here, a voltage within the plateau region was chosen. Again, only one noble gas was tested for the same reason as in experiment 1. The gas pressure was continously changed from 0 - 0.30 mbar, as the ion currents were registered. The result is shown in figure 4.2.2.
The ion current increases for pressures up to about 0.15 mbar. The reason for this is, of course, that more gas atoms may be ionized. The stagnation, and at even higher pressure the reduction, is mainly due to increasing absorption in the previous cells (the rotary-and diffusion pump chambers) and a decreasing

mean free path for the ions.

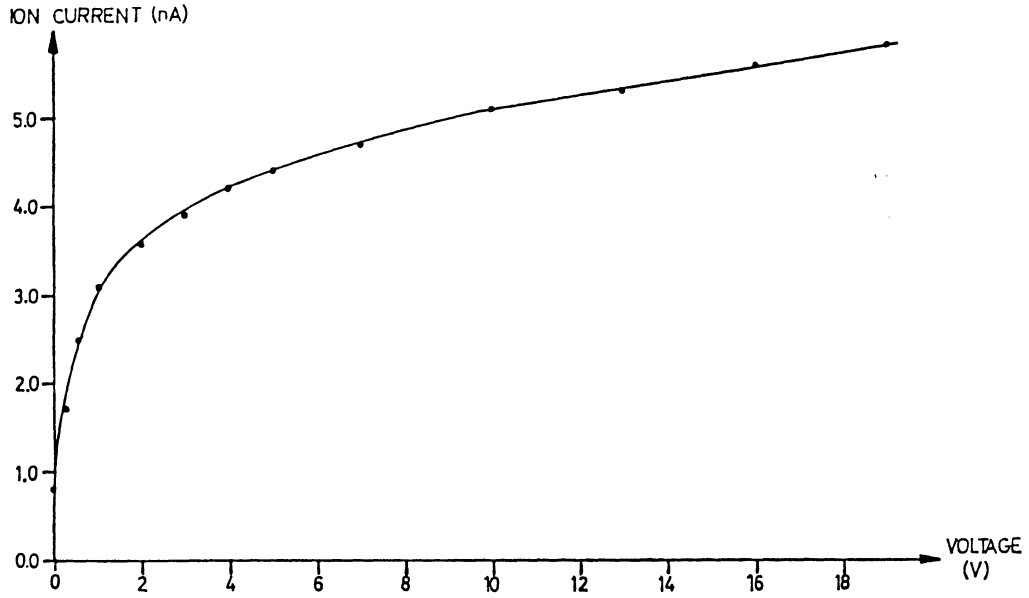

Fig.4.2.1 Ion current versus voltage.The gas pressure was 0.20 mbar (argon).The pulse energy was 0.15 J.

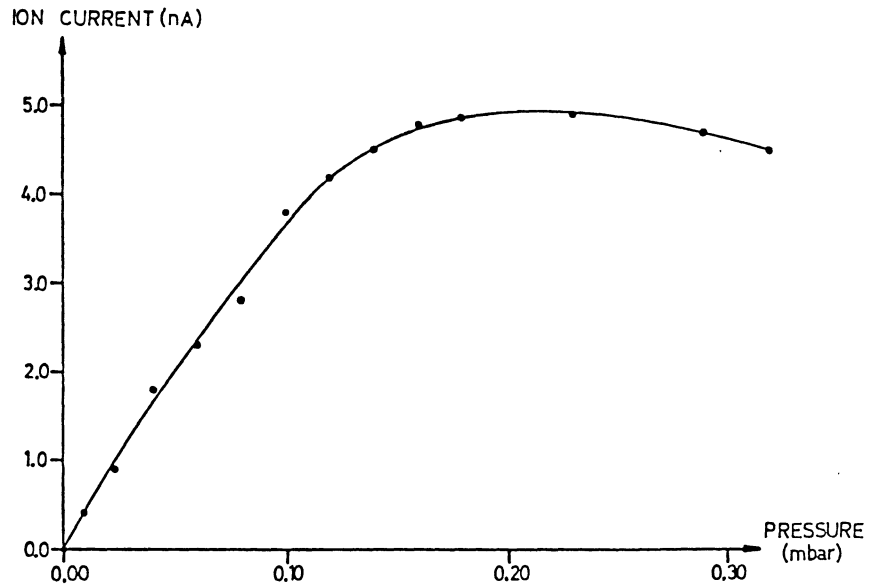

Fig.4.2.2 Ion current versus gas pressure (argon).The voltage between the anode and the cathode was 5 V.The pulse energy was 0.15 J.

Experiment 3:

In this experiment,both voltage and pressure were chosen by taking experiment 1 and 2 in consideration.Three different rare gases were examined (xenon,krypton and argon).The laser pulse energy was continously changed

between 0.25 J and 0.65 J, as the ion currents were registered. The translation from ion current to VUV-photons is described in appendice A3. The result for each gas is shown, respectively, in figures 4.2.3, 4.2.4 and 4.2.5.

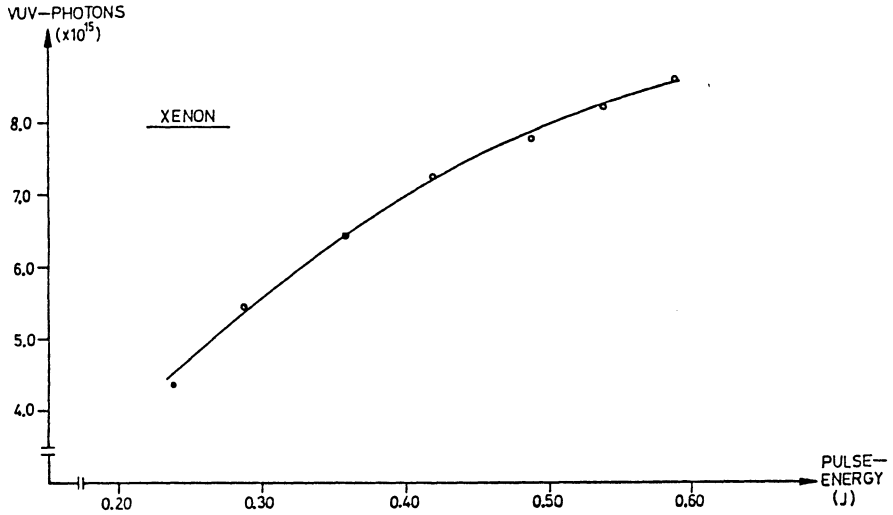

Fig.4.2.3 Number of photons with wavelength 1022 Å, or less, versus pulse energy. The gas pressure was 0.20 mbar (xenon). The voltage between the anode and the cathode was 15 V.

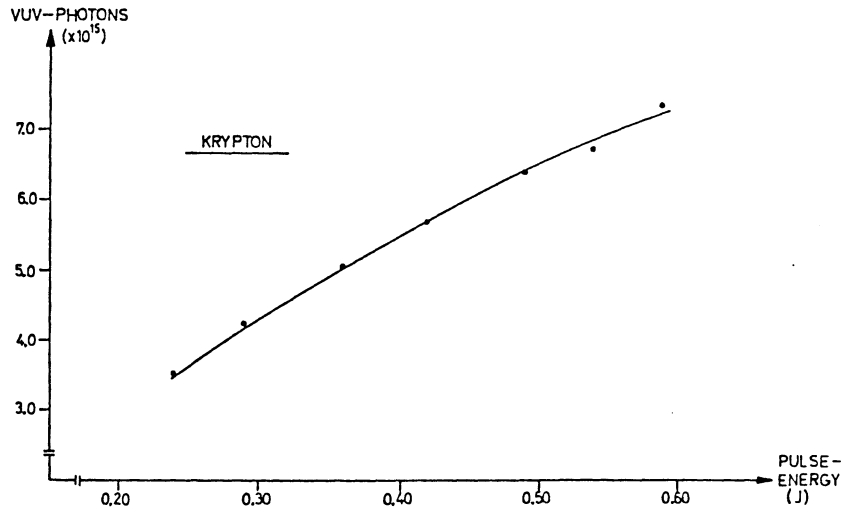

Fig.4.2.4 Number of photons with wavelength 886 Å, or less, versus pulse energy. The gas pressure was 0.20 mbar (krypton). The voltage between the anode and the cathode was 15 V.

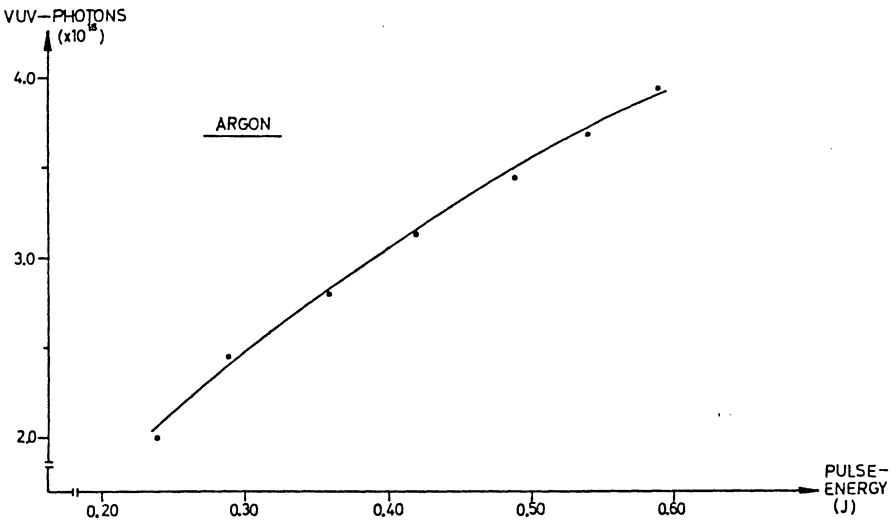

Fig.4.2.5 *Number of photons with wavelength 787 Å, or less, versus pulse energy. The gas pressure was 0.20 mbar (argon). The voltage between the anode and the cathode was 15 V.*

Since, the photoionization potential increases in order Xe - Kr - Ar the number of registered VUV-photons from the plasma decreases in the same order. Noticable is that, when argon was used the number of registered VUV-photons dropped significantly.

5 SUMMARY

The important results from theory and experiments are presented in this subchapter. After each remark is a page reference given.

* A focused Q-switched laser pulse can produce a plasma with a temperature of about 10^5 K in a few nanoseconds (p.3).

* The absorption of laser energy in the plasma is due to the invers bremsstrahlung process (p.3).

* Penetration into the plasma requires that the optical frequency must be higher than the plasma frequency (p.4).

* Optical spectroscopic studies on plasmas show both line and continuum radiation (p.4).

* The continuum radiation consists of bremsstrahlung and recombination radiation (p.5).

* Local thermodynamic equilibrium (LTE) is applicable for a plasma, which is pumped by a Q-switched laser pulse. In case of LTE the electron and ion temperature may be regarded as equal (p.5).

* Recombination radiation probably dominates bremsstrahlung for heavy targets (p.6).

* The best way to construct an absolute intensity detector is by utilizing the principle of photoionization of a rare gas (p.8).

* Continuum radiation strongly dominates line radiation for heavy targets (p.21).

* The number of photons emitted from a plasma which is pumped by a focused 0.5 J laser pulse is of order 10^{16} (p.25).

APPENDICES

A1. Calculation of the power density in the focused laser beam

Our Nd:YAG laser beam may be regarded as a gaussian beam. The theory of gaussian beams is rather complex. Hence, just the results are presented below. The spotdiameter in focus is given by [ref. 6]

$$d = 4\lambda f/\pi D, \qquad (A1.1)$$

where λ, f and D are, respectively, the laser wavelength, lens focal length and laser beam diameter before focusing.

In my case: $\lambda = 1.06\ \mu m$

$f = 0.25\ m$

$D = 0.011\ m$

giving a spotdiameter of 31 μm. The laser pulse duration is 10 ns. If the laser output energy is 0.15 J the corresponding power density becomes $2.0 \times 10^{16}\ W/m^2$.

It may also be of interest to see how the power density alters if we unfocus the laserbeam, with respect to the target. The spotdiameter nearby focus, $d_c(z)$, is given by

$$d_c(z) = d\left(1+\left(\frac{4\lambda z}{\pi d^2}\right)^2\right)^{1/2} \qquad (A1.2)$$

where z is the deviation from the focal length of the lens. Table A1.1 shows the power density for a few different distances from the lens to the target.

Table A1.1 *Power densities at varying focusing*
The laser output energy is 0.15 J.

L (m)	P (W/m^2)
0.230	2.5×10^{13}
0.240	1.0×10^{14}
0.250*	2.0×10^{16}
0.260	1.0×10^{14}
0.270	2.5×10^{13}
0.280	1.1×10^{13}

*)lens focal length

A2 Estimation of the radiation entering the ionization chamber

The plasma radiates energy in a loob as shown in figure A2.1.

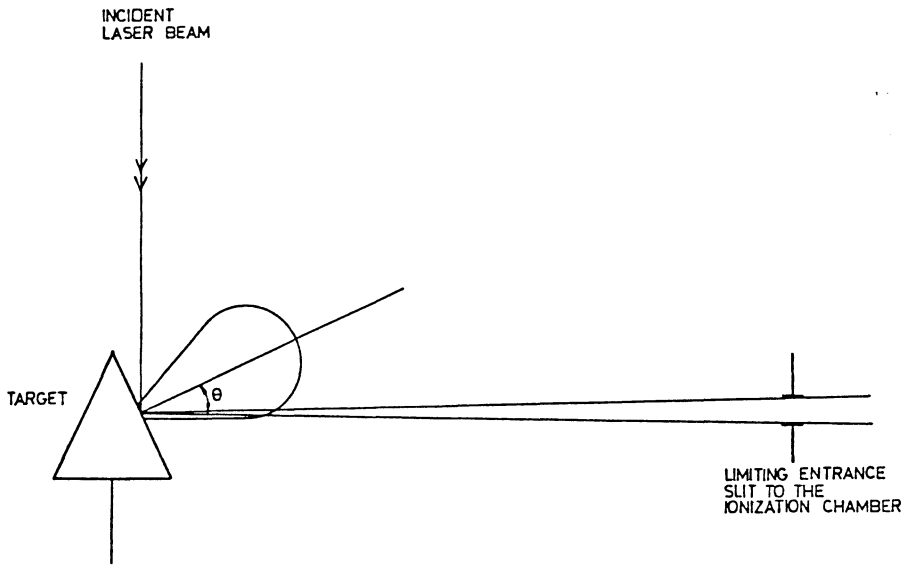

Fig.A2.1 The radiation loob from a plasma

Let us denote the total number of photons, produced in the plasma by Φ_0. It can be shown [Sommerfeld] that

$$I(\Theta)d\Omega \sim \cos^2\Theta d\Omega, \qquad (A2.1)$$

where $I(\Theta)$ is the number of photons emitted per unit of solid angle, and in a direction Θ. Φ_0 must equal $\int_\Omega I(\Theta)d\Omega$, giving

$$\Phi_0 = 2\pi K \int_0^{\pi/2} \cos\Theta^2 \sin\Theta d\Theta = -2/3\pi K \left[\cos^3\Theta\right]_0^{\pi/2} = 2/3\pi K \qquad (A2.2)$$

Hence,

$$I(\Theta)d\Omega = 3\Phi_0/(2\pi)\ \cos^2\Theta d\Omega \qquad (A2.3)$$

In my case $\Theta = 30^0$

$d\Omega = 4.0\times10^{-5}$ Sr

giving the ratio $I(30^0)d\Omega/\Phi_0 = 1.4\times10^{-5}$.

A3 Translation from ion current to VUV-photons

Equation (2.14) in subchapter 2.2 gives the number of photons entering the ionization chamber if the two ion currents i_1 and i_2 are known. Unfortunately, the result is only valid if the absorption coefficients are equal for all wavelengths (or if only one wavelength is present). Figure A3.1 provides the absorption coefficients for the rare gases as a function of wavelength.

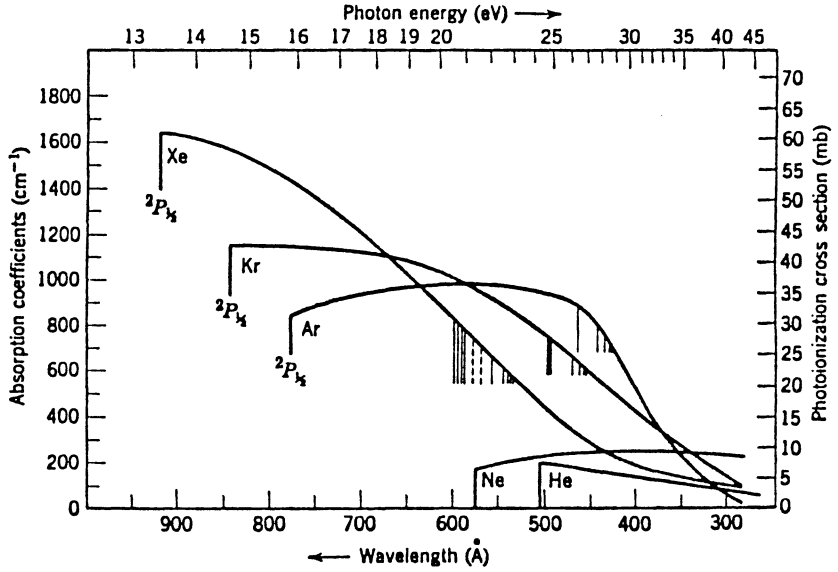

Fig.A3.1 Absorption coefficients for the rare gases as a function of wavelength.The vertical lines indicate positions of discrete structure [taken from ref.5.].

Since, all wavelengths are represented in my case, equation (2.14) is not directly applicable. To make an acceptable estimation of the number of photons produced in the plasma, I followed the procedure presented below:

1) The wavelength scale is divided into 100 Å intervals, in which the absorption coefficient is set to a constant value.

2) In these intervalls is equation (2.11) applicable.

3) The intensity ratio between to adjacent intervals is measured in figure 4.1.1.

The total number of photons may be approximated as follows:

$$I_0 = I(\lambda_1)+I(\lambda_2)+.. \quad ..I(\lambda_n), \qquad \text{(A3.1)}$$

where $I(\lambda_n)$ is the number of photons in interval n, with the centre wavelength λ_n.
Equation (2.11) gives

$$I(\lambda_n) = K(\lambda_n) i_1(\lambda_n), \qquad \text{(A3.2)}$$

where $K(\lambda_n)$ and $i_1(\lambda_n)$ are, respectively, a factor containing the absorption coefficient $\mu(\lambda_n)$ and the induced ion current originating from the photons in interval n.
Combining (A3.1) with (A3.2), and knowing the ratio $C = I(\lambda_n)/I(\lambda_{n+1})$ (measured), gives

$$C = K(\lambda_n) i_1(\lambda_n) / K(\lambda_{n+1}) i_1(\lambda_{n+1}). \qquad \text{(A3.3)}$$

The total ion current is

$$i_1 = i_1(\lambda_1) + i_1(\lambda_2) + \ldots \ldots + i_1(\lambda_n). \qquad \text{(A3.4)}$$

This makes it possible to express i_1 in, say, $i_1(\lambda_1)$.
Since i_1 is measured with the Knick nanoamperemeter, $i_1(\lambda_1)$ is known. If $i_1(\lambda_1)$ is known, then all $i_1(\lambda_n)$ are known. These give all $I(\lambda_n)$. I_0 is then divided by the geometrical factor 1.4×10^{-5}. This gives the total number of photons, produced in the plasma, with wavelengths corresponding to the ionization potential for the rare gas used, or less.

REFERENCES

1) Ready, John F
Effects of high power laser radiation
p. 95-123, 1965

2) Hallstadius, H
Lundberg, H
Generation of coherent vacuum
ultraviolet radiation
Lrap-86

3) Carroll, P. K
Kennedy, E. T
Laserproduced plasmas
Cont. phys. vol. 22, no. 1, p. 61-96, 1981

4) Cooper, J
Plasma spectroscopy
Reports on progress in phys. 1966, vol. 29, p. 36-124

5) Samson, J. A. R
Techniques of vacuum ultraviolet spectroscopy
p. 263-276, 1967

6) Borgström, S
Laserfysik
p. 8. 1-8. 4, 1987